Offset Learning based Channel Estimation for IRS-Assisted Indoor Communication

Zhen Chen*, Hengbin Tang*, Jie Tang*, Xiu Yin Zhang* and Qingqing Wu† Shi Jin‡ and Kai-Kit Wong§
*School of Electronic and Information Engineering, South China University of Technology, Guangzhou, China
† State Key Laboratory of Internet of Things for Smart City, University of Macau, Macau, China
‡School of Electrical and Electronic Engineering, University of Manchester, Manchester, United Kingdom, UK
§Department of Electronic and Electrical Engineering, University College London, UK

***Abstract*—The system capacity can be remarkably enhanced with the help of intelligent reflecting surface (IRS) which has been recognized as a advanced breaking point for the beyond fifth-generation (B5G) communications. However, the accuracy of IRS channel estimation restricts the potential of IRS-assisted multiple input multiple output (MIMO) systems. Especially, for the resource-limited indoor applications which typically contains lots of parameters estimation calculation and is limited by the rare pilots, the practical applications encountered severe obstacles. Former works takes the advantages of mathematical based statistical approaches to associate the optimization issue, but the increasing of scatterers number reduces the practicality of statistical approaches in more complex situations. To obtain the accurate estimation of indoor channels with appropriate piloting overhead, an offset learning (OL)-based neural network method is proposed. The proposed estimation method can trace the channel state information (CSI) dynamically with non-priori information, which get rid of the IRS-assisted channel structure as well as indoor statistics. Moreover, a convolution neural network (CNN)-based inversion is investigated. The CNN, which owns powerful information extraction capability, is deployed to estimate the offset, it works as a offset estimation operator. Numerical results show that the proposed OL-based estimator can achieve more accurate indoor CSI with a lower complexity as compared to the benchmark schemes.**

I. Introduction

Massive multiple-input multiple-output (MIMO) as a promising technology of the fifth-generation (5G) wireless communications systems has received increasing attention in both academia and industry [1], [2]. Although massive MIMO with beamforming has been proved a effective approach to improve the spectral efficiency as well as to boost the system throughput, the inaccurate channel estimation greatly limits its application. The non-line-of-sight (NLOS) links between the transceiver suffer from deep fading and shadowing which is caused by unfavourable propagation conditions.

With the tireless exploration of scientists, intelligent reflecting surface (IRS) has been explored and applied to enhance the coverage and capacity of the wireless communication system with low hardware cost and energy consumption [3]. The IRS works without power supply and can be deployed properly to establish extra links between the access point (AP) and user equipments (UEs) owing to the low-cost and passive advantage of reflecting materials. While the beams are reflecting by the reconfiguring IRS elements those inflected by the radio environment, the received signal power is enhanced and the interference is suppressed. Therefore, a high beamforming gain can be reached [4]. It should be emphasized that the specific reconfiguring method of IRS is to adjusting the phase shifts of IRS elements, furthermore, the higher beamforming gain of IRS is based on the accurate channel state information (CSI) of all links between UEs and APs. In spite of the superior prior works on channel estimation in wireless communication systems, channel estimation of an IRS-assisted wireless communication system is still an arduous difficulty, which is resulted by following reasons. First of all, IRS, a passive device, does not possess any radio frequency chains, that means the IRS can not deal the pilot signal [5], which renders IRS incapable of conventional pilot-aided channel estimation. Secondly, the training process is time restricted, all the adjusting of IRS elements must finish in a very short time. As a result, mobility situation under indoor scenarios e.g. supermarket, commercial towers, shopping mall, may beyond the capacity of IRS. Thence, we devote our passion to develop efficient indoor channel estimation solution for IRS-assisted beyond 5G system.

A. Contributions

IRS has been envisioned as superior and enabling technique to improve the communication condition and signal coverage in the next generation wireless communications. In more detail, deep learning (DL) technique has been introduced into the IRS system. This interdisciplinary research has attracted significant attention recently. Usually, prior works mainly put the focus on the open environment, such as the squares, streets, etc. rather than the indoor condition. As a fact, the micro- or pico-cell are usually deployed in indoor scenarios where the scatter is typically numerous. Moreover, the smart factory scene where the devices are highly dense and served by few APs, is also a typical indoor scenario which is important as the outdoor. In the indoor scenario, rich short-distance scatter path, which yields increased channel dimension, diversity and computation complexity in channel estimation, make the joint optimization of indoor channel estimation and reflection elements of IRS a highly complex problem to tackle with a mathematical-based deterministic approaches. Even worse, the channel status may change intensely with the slight movement of UEs. In order to satisfy the requirement of indoor B5G wireless communication, we proposed a novel channel esti-

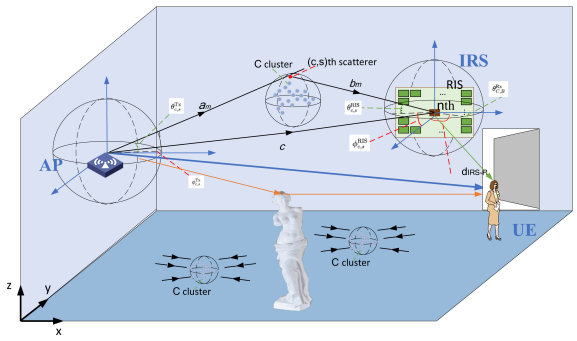

Fig. 1: Generic indoor communication with clusters between AP-IRS and an IRS mounted in the wall.

mation techniques with deep learning architecture to reliably estimate the IRS-assisted channels with a reduced number of pilot overhead in indoor communication scenario. To address the computationally expensive optimization problem with mathematical-based deterministic algorithm, we unroll the iterative procedures of the ADMM-based deterministic algorithm to a supervised model-driven network. Thanks to the DL architecture, all the parameters (e.g., sparse transforms, regularization operator, penalty parameters, etc.) can be trained and learned discriminatingly from the training pairs of pilot signal and estimated signal over the data flow graph.

II. System Model and Problem Formulation

A. IRS-Assisted mmWave MIMO system

The model is based on an IRS-assisted mmWave indoor communication system, in which an AP with N transmit antennas is serving a single-antenna UE. The IRS is consist of an $L \times L$ uniform rectangular array (URA) and it was deployed to assist the communication between the UE and the AP. Taking the complex indoor channel condition into consideration, the widely used clustered statistical MIMO channel model in 3GPP standardization is explore thoroughly [6]. For the requirement in indoor scenario, the clustered statistical MIMO channel model is studied, which is generally used in 3GPP standardization [6]. As shown in Fig. 1, there are M scatterers between the AP and the IRS, while assuming a *LOS* channel link from the IRS to the UE. We assume the UE transmit power as τ, i.e., $\mathbb{E}[|s_b|^2] = \tau$, $\forall t$. Denote a_m, b_m and c as the distances from AP to the m-th scatterer, from the m-th scatterer to the IRS, and from the IRS element to UE, respectively. Thus, the received signal $\hat{\boldsymbol{y}} \in \mathbb{C}^{K\times 1}$ at the UE can be written as

$$\hat{\boldsymbol{y}}_b = \boldsymbol{W}_b \left(\boldsymbol{H}_{UA,b}^H + \boldsymbol{G}\boldsymbol{\Theta}\boldsymbol{H}_{IA}^H\right)\boldsymbol{x}_b + \boldsymbol{n}_b, \tag{1}$$

where $\boldsymbol{H}_{UA} \in \mathbb{C}^{N\times K}$ denotes the channels between the AP and the UE, $\boldsymbol{H}_{IA} \in \mathbb{C}^{L\times K}$ and $\boldsymbol{G} \in \mathbb{C}^{L\times N}$ denote the channels from the AP to the IRS and from the IRS to the UE, respectively. $\boldsymbol{W}_b \in \mathbb{C}^{M\times K}$ denotes antenna selectors. $\boldsymbol{\Theta} \in \mathbb{C}^{L\times L}$ is diagonal phase-shifting matrix of the IRS, which can be expressed as

$$\boldsymbol{\Theta} = \mathrm{diag}\left(\beta_1 e^{j\theta_1}, ..., \beta_L e^{j\theta_L}\right), \tag{2}$$

and $\theta_l \in [0, 2\pi)$, $\beta_l \in [0, 1]$, $l = 1, ..., L$ being the reflection amplitude and phase shift associated with the l-th reflecting element of the IRS, respectively. $\boldsymbol{n}_b \in \mathbb{C}^{M\times 1}$ is the additive white Gaussian noise (AWGN) vector whose entries are with zero mean and variance σ^2.

B. IRS-Assisted channel model

1) AP-IRS Channel: The model assumed that the whole M scatterers are divided into C clusters. Each of cluster is consists of S_c sub-rays for $c = 1, ..., C$, that is $M = \sum_{c=1}^{C} S_c$ and there are sharing the same spatial and temporal distribution characteristics [7]. Then, the AP-IRS channel link $\boldsymbol{H}_{IA} \in \mathbb{C}^{L\times K}$ can be expressed as a clustered model as follows

$$\begin{aligned}\boldsymbol{H}_{IA} &= \boldsymbol{H}_{IA,NLOS} + \boldsymbol{H}_{IA,LOS},\\ &= \gamma \sum_{c=1}^{C}\sum_{s=1}^{S_c} \beta_{c,s}\sqrt{G_e(\theta_{c,s}^{IRS})L_{c,s}^{IRS}}\mathbf{a}(\varphi_{c,s}^{AP})\mathbf{a}(\phi_{c,s}^{IRS}, \theta_{c,s}^{IRS})\\ &+ \boldsymbol{H}_{IA,LOS},\end{aligned} \tag{3}$$

where $\gamma = \sqrt{\frac{1}{\sum_{c=1}^{C} S_c}}$ is a normalization factor used in clustered channel models [6]. $\varphi_{c,s}^{AP}$ is the corresponding azimuth angle-of-arrival (AoA) to the AP; $L_{c,s}^{IRS}$ denotes the path gains of the AP-IRS channel associated with the (c, s)-th propagation path. $\phi_{c,s}^{IRS}$ (or $\theta_{c,s}^{IRS}$) denotes the corresponding angle-of-departure (AoD) of the IRS. $G_e(\theta_{c,s}^{IRS})$ denotes the rotationally symmetric IRS element pattern with the (c, s)-th directed scatterer [8]. Inspired by [8], the cos^q pattern is used to model the reflect arrays of IRS

$$G_e\left(\theta_{c,s}^{IRS}\right) = 2(2q+1)cos^{2q}\left(\theta_{c,s}^{IRS}\right), \quad -\frac{\pi}{2} < \theta_{c,s}^{IRS} < \frac{\pi}{2}, \tag{4}$$

where $2(2q + 1)$ is defined as energy conservation and $q = 0.25G_e(0) - 0.5$ is consistent with in [9]. For the attenuation of the (c, s)-th path, the close-in free space reference distance in the 5G standard protocol is considered to model the frequency-dependent of path loss, which is widely used for the indoor hotspot and urban microcellular scenarios [10]:

$$\begin{aligned}L_{c,s}^{IRS} = &-20\log_{10}\left(\frac{4\pi}{\lambda}\right) - X_\sigma\\ &- 10n\left(1 + \varpi\left(\frac{f - f_0}{f_0}\right)\right)\log_{10}(d_{c,s}),\end{aligned} \tag{5}$$

where $d_{c,s} = a_c + b_{c,s}$ denotes the length of the (c, s)-th path, and f_0 denotes a fixed reference frequency of the path loss model, ϖ denotes a system parameter, and $X_\sigma \sim \mathcal{N}(0, \sigma^2)$ is the shadow fading factor in dB, which is the same in [11].

On the other hand, there is an existing *LOS* link from the AP to IRS in (3). To this end, the *LOS* channel link attenuation for each sub-ray is introduced from the AP to IRS, which is calculated by

$$\boldsymbol{H}_{IA,LOS} = \Gamma(d_{IRS})\sqrt{G_e(\theta_{LOS}^{IRS})L_{LOS}^{IRS}}\eta\mathbf{a}(\varphi_{IRS}^{AP})\mathbf{a}(\phi_{LOS}^{IRS}, \theta_{LOS}^{IRS})^H, \tag{6}$$

where L_{LOS}^{IRS} denotes the attenuation of the *LOS* link to be calculated with (5), $G_e(\theta_{LOS}^{IRS})$ denotes the corresponding channel gain of IRS, $\eta \sim \mathcal{U}[0, 2\pi]$ is the random phase and $\mathbf{a}(\varphi_{IRS}^{AP})$ (or $\mathbf{a}(\phi_{LOS}^{IRS}, \theta_{LOS}^{IRS})$) denotes the array response of the AP (or IRS). $\Gamma(d_{c,s})$ is a Bernoulli random variable taking values between 0 and 1. Let $p(\Gamma(d_{IRS}))$ be the frequency independent *LOS* probability. Then, we can resort to the 5G channel model [10] to achieve

$$p(\Gamma(d_{IRS})) = \begin{cases} 1 & d_{c,s} \leq 1.2 \\ e^{-\frac{d_{c,s}-1.2}{4.7}} & 1.2 < d_{c,s} \leq 6.5 \\ 0.32e^{-\frac{d_{c,s}-6.5}{32.6}} & d_{c,s} > 6.5. \end{cases} \quad (7)$$

According to (7), it is not difficult to notice that if the distance between the IRS and UE is less 4.5m, an *LOS* link probability of greater than 50% is achieved. Therefore, this distance generally takes place in indoor communication.

2) IRS-UE Channel: In indoor communication scenarios, assuming that the IRS is close to the UE and there is a clear *LOS* channel link between the IRS and the UE without noticeable non-*LOS* (*NLOS*) channel link. To be specific, the IRS-UE channel $\boldsymbol{G}$ can be formulated as

$$\boldsymbol{G} = \sqrt{G_e\left(\theta_{UE}^{IRS}\right) L_{LOS}^{IRS\text{-}R}} e^{j\eta} \mathbf{a}(\phi_{UE}^{IRS}, \theta_{UE}^{IRS}) \mathbf{a}(\varphi_{LOS}^{UE})^H, \quad (8)$$

where $\mathbf{a}(\phi_{UE}^{IRS}, \theta_{UE}^{IRS})$ denotes the array response of IRS to be calculated by the azimuth and elevation departure angles ϕ_{UE}^{IRS} and θ_{UE}^{IRS}, $\mathbf{a}(\varphi_{LOS}^{UE})$ denotes the array response of the UE, and $L_{LOS}^{IRS\text{-}R}$ denotes the attenuation of the path loss along with channel related parameters between the IRS and UE that is obtained with (5). The gain of IRS $G_e(\theta_{UE}^{IRS})$ with respect to the departure elevation angle θ_{UE}^{IRS} is obtained by (4).

3) AP-UE Channel: As shown in [10], if the distance from the UE to the IRS is less than the correlation distance, there are common clusters in indoor environments. This motives us to model the channel between AP and the UE by exploiting shared clusters [12]. Therefore, the AP-UE channel can be expressed as

$$\boldsymbol{H}_{UA,b} = \gamma \sum_{c=1}^{C} \sum_{s=1}^{S_c} \beta_{c,s} \sqrt{G_e(\theta_{c,s}^{UA}) L_{c,s}^{IRS}} \mathbf{a}(\varphi_{c,s}^{UE}) \mathbf{a}(\phi_{c,s}^{IRS}, \theta_{c,s}^{IRS}), \quad (9)$$

where the parameters γ, C, $L_{c,s}^{IRS}$ and S_c are defined as in (3) and the common clusters are considered for the AP-UE channel and the AP-IRS channel. By turning off the IRS reflecting elements, i.e., $\beta = 0$, the channel $\boldsymbol{H}_{UA,b}$ can be estimated by considered the conventional estimation schemes.

Combining (3), (8) with (9) and assuming the pilot signal $\mathbb{E}[\boldsymbol{s}_b \boldsymbol{s}_b^H] = \boldsymbol{I}$, we can further obtain (1) by using the vectorization operation

$$\boldsymbol{y}_b = (\boldsymbol{P}_b \boldsymbol{s}_b \otimes \boldsymbol{W}_b) \mathrm{vec}(\boldsymbol{H}_b) + \boldsymbol{n}_b = \boldsymbol{\Phi} \boldsymbol{h}_b + \boldsymbol{n}_b, \quad (10)$$

where $\boldsymbol{y}_b = \hat{\boldsymbol{y}}_b - \boldsymbol{\Phi} \boldsymbol{H}_{UA,b}$, $\boldsymbol{\Phi} = (\boldsymbol{P}_b \boldsymbol{s}_b) \otimes \boldsymbol{W}_b$ is the measurement matrix, $\boldsymbol{h}_b = \mathrm{vec}(\boldsymbol{H}_b) = \mathrm{vec}(\boldsymbol{H}_{IA} \boldsymbol{\Theta} \boldsymbol{G})$ is the vectorized channel. According to the definition of $\boldsymbol{H}_b$, the cascade channel $\boldsymbol{H}_b$ can be further represented as

$$\begin{aligned} \boldsymbol{H}_b &= \boldsymbol{H}_{IA}^H \boldsymbol{\Theta} \boldsymbol{G} \\ &\overset{(a)}{=} (\boldsymbol{H}_{IA,NLOS} + \boldsymbol{H}_{IA,LOS}) \boldsymbol{\Theta} \boldsymbol{G} \\ &= \left(\boldsymbol{F}_{LOS,1} \boldsymbol{\Gamma}_{LOS} \boldsymbol{F}_{LOS,2}^H + \boldsymbol{F}_{NLOS,1} \boldsymbol{\Gamma}_{NLOS} \boldsymbol{F}_{NLOS,2}^H\right) \boldsymbol{\Theta} \boldsymbol{R}_1 \boldsymbol{\Lambda}_G \boldsymbol{R}_2^H \end{aligned} \quad (11)$$

where (a) is from (3), $\boldsymbol{F}_{NLOS,1}$ and $\boldsymbol{F}_{NLOS,2}$ denote the overcomplete matrices and each of its columns has a form of $\mathbf{a}(\varphi_{c,s}^{UE})$ and $\mathbf{a}(\phi_{c,s}^{IRS}, \theta_{c,s}^{IRS})$, respectively; $\boldsymbol{F}_{LOS,1}$, $\boldsymbol{F}_{LOS,2}$ are defined with each of its columns having a form of $\mathbf{a}(\varphi_{IRS}^{AP})$, and $\mathbf{a}(\phi_{LOS}^{IRS}, \theta_{LOS}^{IRS})$, respectively. $\boldsymbol{R}_1$ and $\boldsymbol{R}_2$ are similarly defined with each of its columns having a form of $\boldsymbol{a}_{IRS,2}(\varphi_{l'})$ and $\boldsymbol{a}_{AP}(\phi_{l'})$, respectively.

By stacking all the subcarriers, the received signal can be given by

$$\boldsymbol{Y} = \boldsymbol{\Phi}_{LOS} \boldsymbol{H}_{LOS} + \boldsymbol{\Phi}_{NLOS} \boldsymbol{H}_{NLOS} + \boldsymbol{N}, \quad (12)$$

where $\boldsymbol{Y} = [\boldsymbol{y}_1, \boldsymbol{y}_2, ..., \boldsymbol{y}_B]^T$, $\boldsymbol{\Phi}_{LOS}$ and $\boldsymbol{\Phi}_{NLOS}$ are the LOS and NLOS link of the measurement matrix, $\boldsymbol{H}_{LOS} = [\boldsymbol{h}_{LOS,1}, \boldsymbol{h}_{LOS,2}, ..., \boldsymbol{h}_{LOS,B}]^T$ is the LOS channel link, $\boldsymbol{H}_{NLOS} = [\boldsymbol{h}_{NLOS,1}, \boldsymbol{h}_{NLOS,2}, ..., \boldsymbol{h}_{NLOS,B}]^T$ is the NLOS channel link and $\boldsymbol{N} = [\boldsymbol{n}_1, \boldsymbol{n}_2, ..., \boldsymbol{n}_B]^T$.

III. Deep learning based cascaded channel estimation

In this section, the channel estimation problem is described and the detailed solution is presented. In [13], an superior method which applying CS theory to reduce pilot overhead is provided to tackle the high-dimensional channel estimation problem under the angular-domain sparsity nature of mmWave MIMO channels. Moreover, many other CS-based algorithms are explored. Inspired by previous work [14], the augmented Lagrangian function of a given CS-based channel model is proposed, which splits the variables into several blocks and can be optimized alternatively. With the introduced auxiliary variable $\boldsymbol{U}$, we rewritten the channel estimation optimization problem (12) as

$$\begin{aligned} \min_{\boldsymbol{H},\boldsymbol{U}} & \frac{1}{2} \|\boldsymbol{Y} - \boldsymbol{\Phi} \boldsymbol{H}\|_F^2 + \lambda_a g_a(\boldsymbol{H}_{LOS}) \\ & + \lambda_b g_b(\boldsymbol{H}_{NLOS}) + \frac{\rho}{2} \|\boldsymbol{H} - \boldsymbol{U}\|_F^2 \\ s.t. \quad & \boldsymbol{U} = \boldsymbol{U}_{LOS} + \boldsymbol{U}_{NLOS}, \end{aligned} \quad (13)$$

where ρ is the penalty parameter and $g_a(\cdot)$, λ_a and λ_b denote regularization parameters, $g_b(\cdot)$ are the regularization function derived from the prior knowledge, such as l_p-norm ($0 \leq p \leq 2$).

ADMM has proven to be an excellent variable splitting algorithm to address the optimization of ill-posed inversion problem (13) with convergence guarantee. But the iterative processes to obtain λ_a and λ_b is with highly computational complexity, making it inappropriate to deal with the indoor scenarios. In order to overcome this difficulty, we developed a unfolded architecture of the ADMM-based iterative procedure

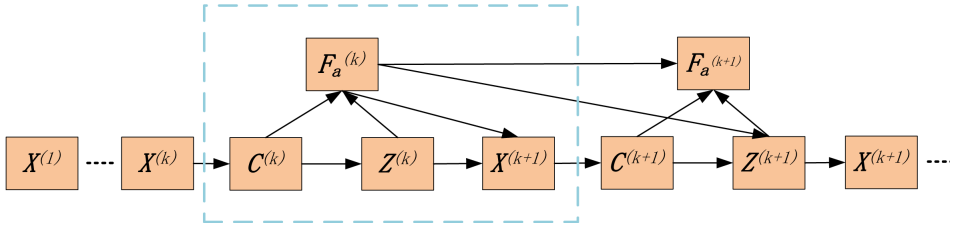

Fig. 2: The data flow graph for the ADMM algorithm

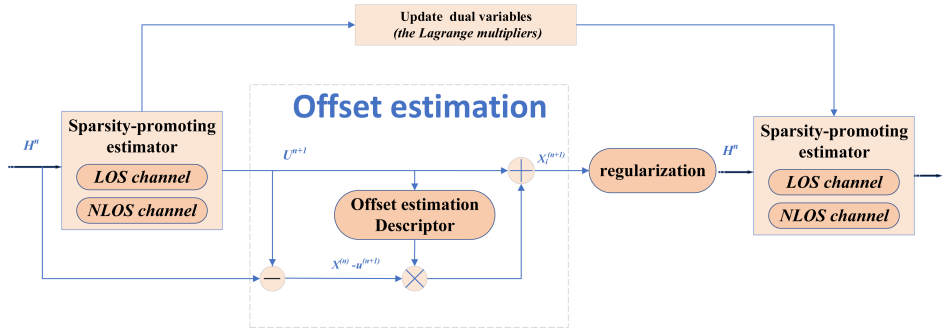

Fig. 3: Overview of the offset learning based indoor channel estimation approach.

to form the framework of the deep learning network. As shown in Fig. 2, it can be observed that each nodes of the graph corresponding to different operations in ADMM, and directed edges corresponding to the data flows between operations. it follows that the k-th stage of the data flow graph corresponds to the k-th iteration of ADMM algorithm.

With the guidance of ADMM framework, a linear offset estimation module to ADMM for channel offset estimation processing can be designed. As a result, the solution to the problem in (13) can be written as follows:

$$\begin{cases} \boldsymbol{H}^{(k+1)} = \arg\min\limits_{\boldsymbol{H}} \dfrac{1}{2}\left\|\boldsymbol{Y}-\boldsymbol{\Phi}\boldsymbol{H}\right\|_F^2 + \dfrac{\rho}{2}\left\|\boldsymbol{H}-\boldsymbol{H}_t^{(k)}\right\|_F^2, \\ \boldsymbol{H}_{LOS}^{(k+1)} = \arg\min\limits_{\boldsymbol{H}_{LOS}} \dfrac{1}{2}\left\|\boldsymbol{H}^{(k+1)}-\boldsymbol{H}_{LOS}-\boldsymbol{F}_a^{(k)}\right\|_F^2 + \lambda_a g_a(\boldsymbol{H}_{LOS}), \\ \boldsymbol{H}_{NLOS}^{(k+1)} = \arg\min\limits_{\boldsymbol{H}_{NLOS}} \dfrac{1}{2}\left\|\boldsymbol{H}^{(k+1)}-\boldsymbol{H}_{NLOS}-\boldsymbol{F}_b^{(k)}\right\|_F^2 + \lambda_b g_b(\boldsymbol{H}_{NLOS}), \\ \boldsymbol{H}_t^{(k+1)} = \boldsymbol{U}^{(k+1)} + \mathcal{T}^{(k+1)} \otimes \left(\boldsymbol{H}^{(k+1)} - (\boldsymbol{H}_{LOS}^{(k+1)} + \boldsymbol{H}_{NLOS}^{(k+1)})\right) \\ \boldsymbol{F}_a^{(k+1)} = \boldsymbol{F}_a^{(k)} + \varrho_a\left(\boldsymbol{H}^{(k)} - \boldsymbol{H}_{LOS}^{(k+1)}\right), \\ \boldsymbol{F}_b^{(k+1)} = \boldsymbol{F}_b^{(k)} + \varrho_b\left(\boldsymbol{H}^{(k)} - \boldsymbol{H}_{NLOS}^{(k+1)}\right), \end{cases} \tag{14}$$

where $\boldsymbol{F}_a$ and $\boldsymbol{F}_b$ are dual variables (the Lagrange multipliers) adding the constraints of (13) to the cost function, $\mathcal{T}$ is the offset descriptor controlled by a parameter V (Details are described in Appendix A), $\boldsymbol{H}_t^{(k)}$ is the k-th iteration of the offset estimation result, $\otimes$ is a Kronecker product operation. It should be noticed that typically the optimization problem (14) needs to run dozens of iterations to achieve a satisfactory estimation accuracy. Furthermore, it is challenging to determine the shrinkage operator for the general regularization functions $g_a(\cdot)$ and $g_b(\cdot)$. To alleviate these difficulties, we will design an ADMM-based deep learning framework to discriminatingly learn all the above transforms, offset descriptor, regularization functions and shrinkage operators. Theoretically, the channel estimation accuracy can be enhanced by employing the OLNN-net, so as to optimize the parameters in OLNN-net.

As shown in Fig. 3, there are four main modules in our proposed deep learning framework: a sparsity-promoting estimation module, dual variables module, an offset estimation module and a regularization module. The descriptor $\mathcal{T}$ in offset estimation module actually works as a special filter, which filters out undesired feature of the residual channel and keeps the desired channel. Finally, the estimated channel will possess the expected feature of the indoor scattering channel. To well-described and analyze this framework, the k-th stage of the proposed OLNN is provided as an example to depict four types of modules as follows.

a) United Layer ($\boldsymbol{U}^{(n,k)}$): The inputs of this layer are $\boldsymbol{U}^{(n,k-1)}$, $\boldsymbol{H}^{(n)}$ and $\boldsymbol{C}_2^{(n,k)}$. The corresponding output result is expressed as

$$\boldsymbol{U}^{(n,k)} = \mu_1^{(n,k)}\boldsymbol{U}^{(n,k-1)} + \mu_2^{(n,k)}\boldsymbol{H}^{(n)} - \boldsymbol{C}_2^{(n,k)}, \tag{15}$$

where the initial value of $\boldsymbol{U}^{(n,1)}$ is $\boldsymbol{H}^{(n)}$.

b) Convolution Layer ($\boldsymbol{C}_1^{(n,k)}$): The input of this layer is $\boldsymbol{U}^{(n)}$ and corresponding the output result can be given by

$$\boldsymbol{C}_1^{(n,k)} = \boldsymbol{w}_1^{(n,k)} * \boldsymbol{U}^{(n,k)} + \boldsymbol{b}_1^{(n,k)}. \tag{16}$$

c) Nonlinear Transform Layer ($\boldsymbol{S}^{(n,k)}$): $\boldsymbol{C}_1^{(n,k)}$ is used as the input of this layer, and the corresponding output result can be given by

$$\boldsymbol{S}^{(n,k)} = \mathcal{S}_{PF}\left(\boldsymbol{C}_1^{(n,k)}; \left\{p_i, q_i^{(n,k)}\right\}_{i=1}^{N_c}\right), \tag{17}$$

where a piecewise linear function $\mathcal{S}_{PF}(\cdot)$ is determined by a fixed point set $\left\{p_i, q_i^{(n,k)}\right\}_{i=1}^{N_c}$.

d) Convolution Layer ($\boldsymbol{C}_2^{(n,k)}$) By calculating (17), the corresponding result $\boldsymbol{S}^{(n,k)}$ can be used as the input of this layer, and the output of this layer is expressed as

$$\boldsymbol{C}_2^{(n,k)} = \boldsymbol{w}_2^{(n,k)} * \boldsymbol{S}^{(n,k)} + \boldsymbol{b}_2^{(n,k)}. \tag{18}$$

1) Regularization Module ($\boldsymbol{Z}_{NLOS}^{(k)}$): Since the signal power of the *NLOS* links are generally weaker than *LOS* link, the deconvolution module is used to learn the parameters by exploiting the learnable Wiener Filtering layer [15]. In case of multiple regularization kernels, we formulate the *NLOS* links objective function as:

$$\boldsymbol{H}_{NLOS}^{(k+1)} = \arg\min_{\boldsymbol{H}_{NLOS}} \frac{1}{2} \left\| \boldsymbol{H}^{(k+1)} - \boldsymbol{H}_{NLOS} - \boldsymbol{F}_b^{(k)} \right\|_F^2 + \lambda_b \|\mathcal{G}\boldsymbol{H}_{NLOS}\|_2^2 \tag{19}$$

where $\mathcal{G}$ denotes the multiple regularization kernel that plays the role of multiple regularizer filters.

2) Offset Estimation Module ($\boldsymbol{R}^{(n)}$): The inputs of this module have two sets $\boldsymbol{U}^{(n)}$, $\boldsymbol{H}^{(n)}$, and the corresponding output result is given by

$$\boldsymbol{H}_t^{(n)} = \boldsymbol{U}^{(n)} + \mathcal{T}^{(n)} \otimes \left(\boldsymbol{H}^{(n)} - (\boldsymbol{H}_{LOS}^{(n)} + \boldsymbol{H}_{NLOS}^{(n)}) \right), \tag{20}$$

where $\mathcal{T}^{(n)}$ denotes offset operator at the n-th of stage.

3) Dual Variables Operation Module ($\boldsymbol{F}^{(n)}$): This module aims to update the variables $\boldsymbol{F}_a$ and $\boldsymbol{F}_b$. The outputs of this layer are

$$\begin{aligned} \boldsymbol{F}_a^{(k+1)} &= \boldsymbol{F}_a^{(k)} + \varrho_a \left(\boldsymbol{H}^{(k)} - \boldsymbol{H}_{LOS} \right) \\ \boldsymbol{F}_b^{(k+1)} &= \boldsymbol{F}_b^{(k)} + \varrho_b \left(\boldsymbol{H}^{(k)} - \boldsymbol{U}_{NLOS} \right) \end{aligned} \tag{21}$$

IV. Simulation Results

In this section, we take Monte Carlo simulations on several key indicators with the IRS-assisted deep channel estimator under the indoor communication scenario. The performance will be provided after the description of OLNN-based network framework simulation parameters. Then, the IRS-assisted deep channel estimator will be comprehensively explored.

A. Simulation Prerequisites

As in a typical IRS-assisted indoor communication scenario, the AP is equipped with $N_t = 36$ antennas and the IRS is equipped with 36 reflecting elements. There are two operating frequencies, that is 28 and 73 GHz. They are adapted to verify the feasibility and validity of the proposed OLNN. At the same time, there are averaging 20000 independent Monte Carlo realizations for each simulation to obtain the simulation result. To adequately collect the training samples, different direction of unit signals are generated from the transmitter to the corresponding received signals. Besides,for each signal to noise ratio (SNR) level, the dataset involved 150000 examples for training and 20000 samples for validation. Following the rules in [9], the IRS element gain $G_e(0)$ is calculated from $G_e(0) = 4\pi A_e(0)/\lambda^2$, where the physical area of an IRS element is given by $A_e(0) = (\lambda/2)^2$.

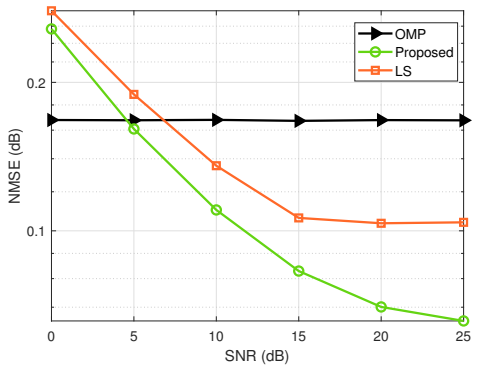

Fig. 4: (a) NMSE performance of LS, OMP and OLNN estimators.

In the first simulation, the performance of proposed OLNN estimator is evaluated for two channel models, namely the LS estimator in [16] and OMP [17]. Fig. 4 depicts the impact of the SNR to NMSE of all considered estimation techniques in the IRS-assisted indoor system. We investigate the NMSE of the proposed OLNN scheme against the SNR levels, where the training sequences $L = 120$. From Fig. 4, it is also evident that the proposed OLNN generally achieves better performance than the OMP and LS channel estimators. In particular, the proposed OLNN scheme substantially improves the estimation performance in terms of the NMSE value compared with the LS, which benefits from the offset learning-based module that can learn the channel error in indoor scenarios. We can conclude that the proposed OLNN scheme is an efficient channel estimation approach, compared with the conventional LS or OMP techniques. This numerical results further indicate that the proposed OLNN is a promising technology for ensuring the reliability of the IRS-assisted indoor system.

To show the effect of number of clusters on the IRS-assist channel estimation, we also conduct the achievable rates of different schemes versus the number of channel clusters in Fig. 5. It is observed that there exists a tradeoff between the the precision of IRS-assist channel estimation and training overhead. This is because a small number of clusters M is not sufficiently accurate for achieving high gain of IRS-based channel, while too many clusters results in computationally expensive in channel estimation process. Moreover, it is observed that the proposed channel estimator with the operating frequencies at 73Hz are slightly better than the 28Hz, at the same number of clusters. It is worth noting that the proposed scheme with OLNN-based framework can effectively escape computing both system memory and time cost.

Finally, we conduct the NMSE performance of the channel estimation in different number of the transmit antennas N_t. According to Fig. 6, the NMSE values of the channel estimation are reducing with the increasing number of ploits, and it becomes stable gradually until the number of pilots are sufficiently large. This indicates that the channel estimation

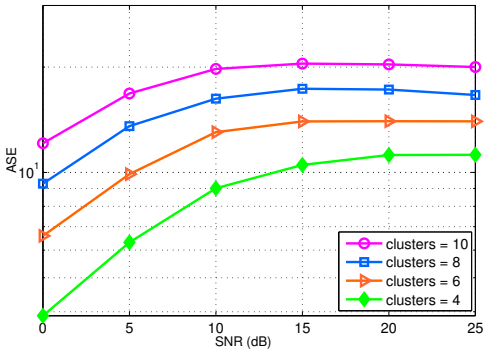

(a)

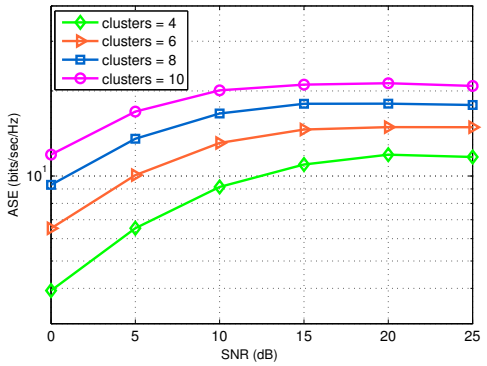

(b)

Fig. 5: (a) NMSE performance against the number of clusters at 73 GHz; (b) NMSE performance against the number of clusters M at 28 GHz.

can be improved when introducing longer training sequences. In addition, one can observe significant improvement of the proposed OLNN by increasing the number of transmit antennas N_t.

V. Conclusion

In this paper, an OL-based neural network is proposed to estimate CSI of an IRS-assisted mmWave MIMO system. The OL-based neural network is integrated into the proposed network framework to tackle the indoor environment. The proposed network architecture is derived from ADMM, which unrolls the iterative procedures to a supervised model-driven network. Theoretical and simulation analysis demonstrate that in the constructed indoor 5G system, the proposed channel estimator exhibits superior performance compared to LS and OMP estimators without any prior knowledge of the IRS-assisted channel and pilot contamination. With the same pilot overhead, the proposed OLNN has an obviously improved accuracy compared with existing algorithms.

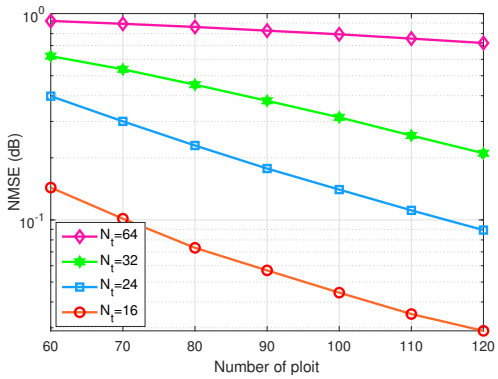

Fig. 6: (a) NMSE performance against the number of ploit at 73GHz.

References

[1] B. Li, D. Zhu, and P. Liang, "Small cell in-band wireless backhaul in massive MIMO systems: A cooperation of next-generation techniques," *IEEE Transactions on Wireless Communications*, vol. 14, no. 12, pp. 7057–7069, 2015.

[2] E. G. Larsson, O. Edfors, F. Tufvesson, and T. L. Marzetta, "Massive MIMO for next generation wireless systems," *IEEE Communications Magazine*, vol. 52, no. 2, pp. 186–195, 2014.

[3] Q. Wu and R. Zhang, "Towards smart and reconfigurable environment: Intelligent reflecting surface aided wireless network," *IEEE Communications Magazine*, vol. 58, no. 1, pp. 106–112, 2020.

[4] Q. Wu and R. Zhang, "Intelligent reflecting surface enhanced wireless network via joint active and passive beamforming," *IEEE Transactions on Wireless Communications*, vol. 18, no. 11, pp. 5394–5409, 2019.

[5] Z. Q. He, H. Liu, X. Yuan, Y. J. A. Zhang, and Y. C. Liang, "Semi-blind cascaded channel estimation for reconfigurable intelligent surface aided massive MIMO." [Online]. Available:https://arxiv.org/abs/2101.07315. dec., 2021.

[6] "3GPP TR 38.901 V16.1.0 - study on channel model for frequencies from 0.5 to 100 ghz," 2019.

[7] I. A. Hemadeh, K. Satyanarayana, M. El-Hajjar, and L. Hanzo, "Millimeter-wave communications: Physical channel models, design considerations, antenna constructions, and link-budget," *IEEE Communications Surveys and Tutorials*, vol. 20, no. 2, pp. 870–913, 2018.

[8] P. Nayeri, F. Yang, and A. Z. Elsherbeni, *Reflectarray Antennas: Theory, Designs, and Applications*. 2018.

[9] S. W. Ellingson, "Path Loss in Reconfigurable Intelligent Surface-Enabled Channels." [Online]. Available:https://arxiv.org/pdf/1912.06759.pdf. dec., 2019.

[10] "5G channel model for bands up to 100 GHz." [Online]. Available:http://www.5gworkshops.com/5GCMSIG_White\%20Paper_r2dot3.pdf. Dec., 2016.

[11] T. S. Rappaport, G. R. MacCartney, M. K. Samimi, and S. Sun, "Wideband millimeter-wave propagation measurements and channel models for future wireless communication system design," *IEEE Transactions on Communications*, vol. 63, no. 9, pp. 3029–3056, 2015.

[12] M. Alonzo, S. Buzzi, A. Zappone, and C. DElia, "Energy-efficient power control in cell-free and user-centric massive MIMO at millimeter wave," *IEEE Transactions on Green Communications and Networking*, vol. 3, no. 3, pp. 651–663, 2019.

[13] Z. Gao, L. Dai, S. Han, C. I, Z. Wang, and L. Hanzo, "Compressive sensing techniques for next-generation wireless communications," *IEEE Wireless Communications*, vol. 25, no. 3, pp. 144–153, 2018.

[14] Z. Chen, C. Huang, and S. Lin, "A new sparse representation framework for compressed sensing MRI," *Knowledge-Based Systems*, vol. 188, p. 104969, 2020.

[15] R. M. Umer, G. L. Foresti, and C. Micheloni, "Deep super-resolution network for single image super-resolution with realistic degradations," *the 13th International Conference*, pp. 1–10, 2019.

[16] D. Mishra and H. Johansson, "Channel estimation and low-complexity beamforming design for passive intelligent surface assisted MISO wireless energy transfer," in *2019 IEEE International Conference on Acoustics, Speech and Signal Processing (ICASSP)*, pp. 4659–4663, 2019.

[17] K. Venugopal, A. Alkhateeb, N. Gonzlez Prelcic, and R. W. Heath, "Channel estimation for hybrid architecture-based wideband millimeter wave systems," *IEEE Journal on Selected Areas in Communications*, vol. 35, no. 9, pp. 1996–2009, 2017.